Supporting Information

Charge injected proton transfer in transistors based on extended and truncated indigo derivatives

Kazuho Ikeda, Dongho Yoo, Ryu Nishikawa, Tadashi Kawamoto, and Takehiko Mori *

Department of Materials Science and Engineering, Tokyo Institute of Technology, O-okayama 2-12-1, Meguro-ku, Tokyo 152-8552, Japan. E-mail: mori.t.ae@m.titech.ac.jp

Synthesis

All commercial chemicals and solvents were used without further purification. The data of Nuclear Magnetic Resonance spectrum (NMR) and Mass spectrum (MS) were obtained with a JEOL JNM-AL300 spectrometer and JEOL JMS-Q1050GC mass spectrometer, respectivery.

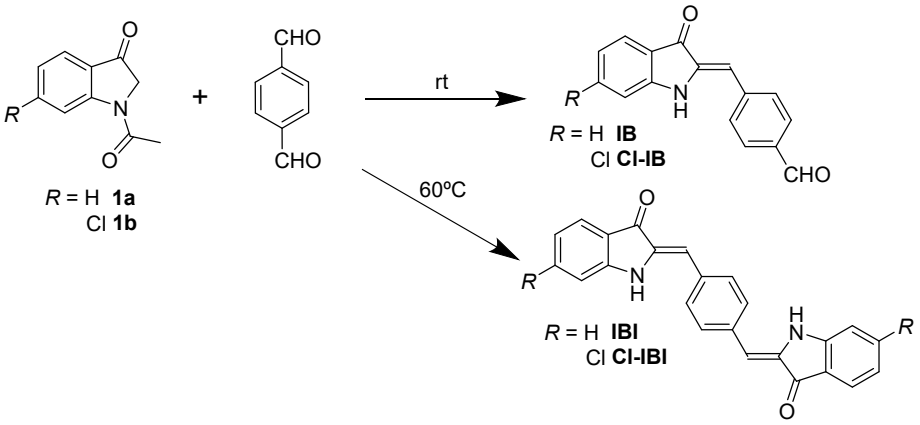

IB: 91 mg of **1a** (0.52 mmol) and 70 mg terephthalaldehyde (0.52 mmol) were dissolved in 10 mL *N*,*N*-dimethylformamide (DMF) under an argon atmosphere. To the resulting solution, 2.0 ml triethylamine was added and the mixture was stirred for 12 h. Water was added to the reacting mixture, and the suspension was filtered. The product was purified by recrystallization from methanol to afford 15 mg of **IB** (0.062 mmol, yield 12%) as an orange solid. EI-HRMS: Calcd. for $[M]^+$ 249.0790, Found 249.0795. ^{1}H NMR (400 MHz, DMSO, 25°C): δ 10.08 (s, 1H), 10.02 (s, 1H), 7.95 (m, 4H), 7.60 (m, 2H),6.95 (t, J = 7.3 Hz, 1H), 6.64 (s, H).

IBI:[22] 210 mg of **1a** (1.2 mmol) and 70 mg terephthalaldehyde (0.52 mmol) were

dissolved in 3.0 mL DMF under an argon atmosphere. To the resulting solution, 2.0 ml triethylamine was added and stirred at 60°C for 24 h. After cooled to room temperature, the resulting mixture was filtered to afford 88 mg of **IBI** (0.24 mmol, yield 47%) as a purple solid. EI-HRMS: Calcd. for $[M]^+$ 364.1212, Found 364.1207. ^{1}H NMR (400 MHz, DMSO, 25°C): δ 10.06 (s, 2H), 8.20 (m, 2H), 7.65 (m, 6H), 7.14 (m, 2H),6.90 (t, J = 6.8 Hz, 2H), 6.56 (s, 2H).

Cl-IB: 60 mg of **1b** (0.29 mmol) and 39 mg terephthalaldehyde (0.29 mmol) were dissolved in 10 mL DMF under an argon atmosphere. To the resulting solution, 2.0 ml triethylamine was added and the mixture was stirred for 12 h. Water was added to the reacting mixture, and the suspension was filtered. The product was purified by recrystallization from methanol to afford 36 mg **Cl-IB** (0.13 mmol, yield 44%) as an orange solid. EI-HRMS: Calcd. for $[M]^+$ 283.0400, Found 283.0394. ^{1}H NMR (400 MHz, DMSO, 25°C): δ 10.08 (s, 1H), 10.02 (s, 1H), 7.95 (m, 4H), 7.62 (m, 1H),6.97 (t, J = 7.0 Hz, 1H), 6.69 (s, H).

Cl-IBI: 102 mg of **1b** (0.49 mmol) and 25 mg terephthalaldehyde (0.19 mmol) were dissolved in 3.0 mL DMF under an argon atmosphere. To the resulting solution, 3.0 ml triethylamine was added and stirred at 60°C for 24 h. After cooled to room temperature, the resulting mixture was filtered to afford 10 mg of **Cl-IBI** (0.023 mmol,

yield 12%) as a purple solid. ESI-HRMS: Calcd. for $[M]^+$ 431.0360, Found 431.0351.

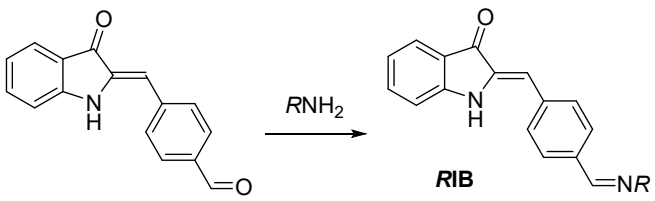

C_nIB: 100 mg of **1a** (0.41 mmol) and 24 mg alkylamine (0.41 mmol) were dissolved in 40 mL ethanol and the mixture was stirred for 24 h. Water was added to the reacting mixture, and the suspension was filtered to afford **C_nIB** as an orange solid.

C_3IB: Orange solid (36%). EI-HRMS: Calcd. for $[M]^+$ 290.1419, Found 290.1493. ^{1}H NMR (400 MHz, Chloroform-D, 16°C): δ 10.00 (s, 1H), 8.27 (m, 2H), 7.58 (m, 2H), 7.48 (d, J = 7.6 Hz, 2H), 7.25 (m, 1H), 6.92 (m, 1H), 6.15 (s, 1H),3.60 (t, J = 6.8 Hz, 2H)1.69 (m, 2H), 0.95 (t, J = 6.8 Hz, 3H).

C_6IB: Orange solid (66%). EI-HRMS: Calcd. for $[M]^+$ 332.1889, Found 332.1898. ^{1}H NMR (400 MHz, Chloroform-D, 16°C): δ 10.00 (s, 1H), 8.26 (m, 2H), 7.71 (m, 2H), 7.57 (d, J = 8.0Hz, 2H), 7.47 (t, J = 8.0Hz, 1H),7.00 (m, 1H), 6.83 (m, 1H), 6.12 (s, 1H),3.62 (t, J = 6.9 Hz, 2H),1.69 (m, 2H), 0.88 (t, J = 6.4 Hz, 3H).

C_8IB: Orange solid (42%). EI-HRMS: Calcd. for $[M]^+$ 360.2202, Found 360.2200. ^{1}H NMR (400 MHz, Chloroform-D, 16°C): δ 10.00 (s, 1H), 8.28 (m, 2H), 7.76 (m, 2H), 7.47 (m, 2H), 7.20 (m, 1H),6.97 (m, 1H), 6.83 (m, 1H), 6.20 (s, 1H),3.62 (t, J = 6.9 Hz, 2H),1.68 (m, 2H), 1.26 (m, 10H),0.88 (m, 3H).

EtPhIB: 100 mg of **1a** (0.41 mmol) and 63 mg 2-phenylethylamine (0.41 mmol) were dissolved in 30 mL ethanol and the mixture was stirred for 24 h. Water was added to the reacting mixture, and the suspension was filtered to afford 110 mg of **EtPhIB** (0.31 mmol, yield 76%) as an orange solid. EI-HRMS: Calcd. for $[M]^+$ 352.1576, Found 352.1576. ^{1}H NMR (400 MHz, Chloroform-D, 16°C): δ 10.00 (s, 1H), 8.27 (m, 2H), 7.58 (m, 2H), 7.48 (d, J = 7.6 Hz, 2H), 7.25 (m, 1H), 6.92 (m, 1H), 6.15 (s, 1H),3.60 (t, J = 6.8 Hz, 2H)1.69 (m, 2H), 0.95 (t, J = 6.8 Hz, 3H).

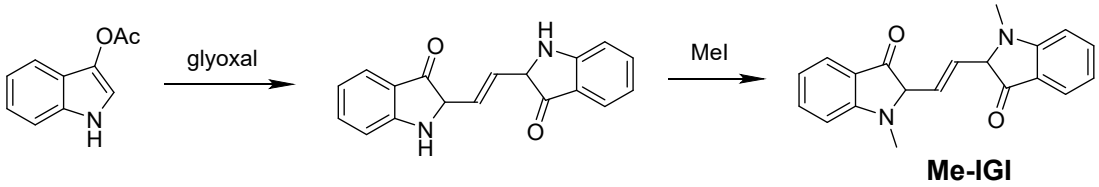

Me-IGI

Me-IGI: 784 mg of indoxyl acetate (4.4 mmol) and 304 mg glyoxal (2.1 mmol) were dissolved in 30 mL ethanol. To the resulting solution, 0.3 ml 6 N HCl was added and the mixture was reflux for 2 h. The resulting mixture was filtered and dissolved in 10 mL DMF. To the resulting solution, 2.2 g methyl iodide (15.5 mmol), 1.0 g calcium carbonate and 0.1 ml water were added and stirred at for 24 h. The solution was evaporated in vacuo and dried. The product was purified by column chromatography on silica gel using CH_2Cl_2 as eluent to afford 279 mg of **Me-IGI** (0.97 mmol, yield 46%) as a purple solid. Mass m/z = 316 [M]. ^{1}H NMR (400 MHz, Chloroform-D, 16°C): δ 8.04 (m, 2H), 7.66 (d t, J = 7.2 Hz, 2H)), 7.45 (t, J = 8.0 Hz, 2H), 7.25 (m, 4H),

6.90 (t, J = 8.0 Hz, 2H), 3.37 (s, 6H).

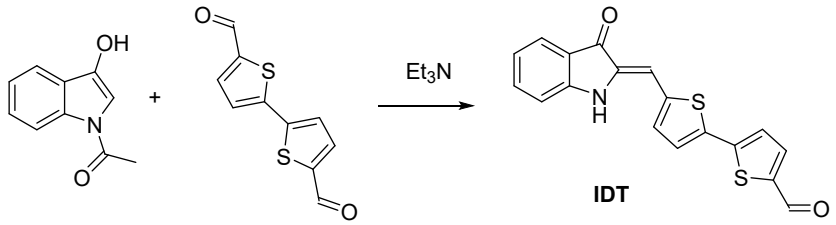

IDT: 190 mg of **1a** (1.1 mmol) and 100 mg 2,2'-bithiophene-5,5'-dicarboxaldehyde (0.45 mmol) were dissolved in 2.0 mL DMF under an argon atmosphere. To the resulting solution, 2.0 ml triethylamine was added and stirred at 60°C for 24 h. After cooled to room temperature, the resulting mixture was filtered to afford 39 mg of **IDT** (0.086 mmol, yield 19%) as a purple solid. EI-HRMS: Calcd. for $[M]^+$ 337.0231, Found 337.0233.

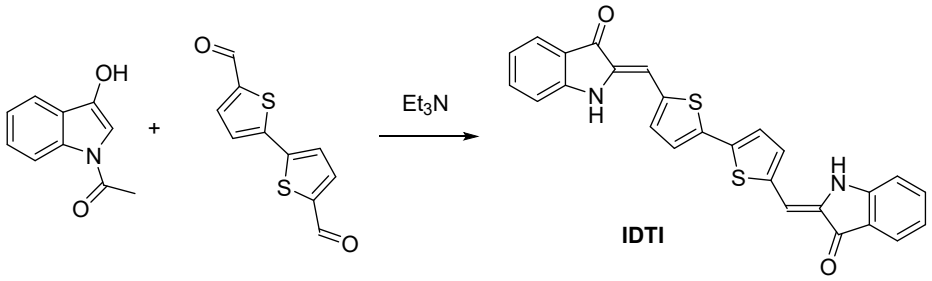

IDTI: 410 mg of **1a** (2.3 mmol) and 51 mg 2,2'-bithiophene-5,5'-dicarboxaldehyde (0.23 mmol) were dissolved in 4.0 mL DMF under an argon atmosphere. To the resulting solution, 4.0 ml triethylamine was added and stirred at 90°C for 72 h. After cooled to room temperature, the resulting mixture was filtered to afford 84 mg **IDTI** (0.19 mmol, yield 80%) as a purple solid. EI-HRMS: Calcd. for $[M]^+$ 452.0653, Found 452.0653.

Cyclic voltammetry (CV) and ultraviolet-visible spectroscopy (UV-Vis)

Reduction potentials were measured by cyclic voltammetry (CV) on an ALS model 701E electrochemical analyzer. The measurement was performed in DMF solution containing 0.1 M tetra-*n*-butylammonium hexafluorophosphate (*n*-$Bu_4N{\cdot}PF_6$) as a supporting electrolyte using a glassy carbon working electrode, a platinum counter electrode, and $Ag/AgNO_3$ electrode as a reference electrode at the scan rate of 50 mV s^{-1} (Fig. 1). The HOMO/LUMO levels were estimated by assuming the ferrocene/ferrocenium energy level to be −4.8 eV under the vacuum level (Table 1).[9] UV-Vis spectra were collected on a Shimadzu UV1800 Spectrophotometer in DMF (Fig. 1) and for evaporated thin films (Fig. S1).

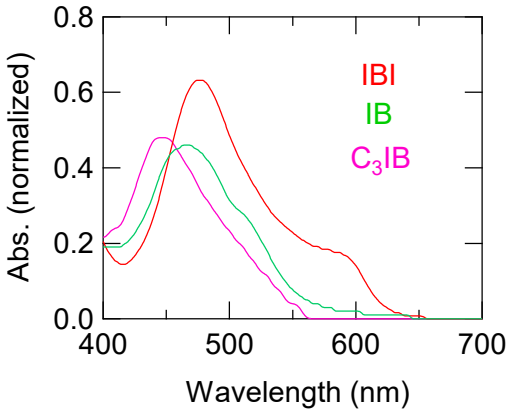

Fig. S1. UV-vis absorption spectra of evaporated films.

DFT calculation

Following our previous investigations,[15,17,18,20,21] the density functional calculations were performed with the B3LYP* functional and TZP basis set using ADF software.[28,S1] Since we have observed considerable difference of energy levels depending on the starting crystal structure analyses in indigo (Table S1),[32,33] E_{HOMO} and E_{LUMO} in parentheses in Table 1 were values after geometry optimization. The enol forms in Table S1 and Fig. S2 were also geometry optimized for the intramolecular 2H transfer. The HOMO and LUMO were basically unchanged in the enol forms (Fig. S2).

For obtaining positions of optical transitions in Fig. 1, the sTD-DFT calculations were carrier out starting from the above optimized molecular structures, with the M06-2X functional and TZP basis set using ADF software.[28,S2]

The resulting first excitation energies E_1 (S_0 -> S_1) were compared with E_{opt} (Table 1), and the enol contribution was estimated from

$$R_{enol} = \frac{E_1(keto) - E_{opt}}{E_1(keto) - E_1(enol)} \qquad \text{(S1)}$$

as listed in Table S2. For the indigo keto form, E_1 = 2.02 eV was near the absorption in polar solvents (2.0 eV/620 nm), and E_{HL} = 2.16 eV was close to 2.29 eV of the gas absorption (540 nm) or 2.10 eV in non polar solvents (590 nm). Since E_1 was not obtained for the intermolecular proton transfer, estimations using E_{HL} instead of E_1 were

also listed in Table S2, where the E_{HL} values of the keto and enol forms were taken from Table S1 (Intra) and Table 3 (Inter). Since E_1 is usually smaller than E_{HL},[S3] the values obtained from E_{HL} tend to overestimate the enol contribution. Although the obtained values are largely dependent on the calculations, thin films show larger enol contributions than solutions, and the truncated **IB** and **C$_n$IB** as well as **IBI** show larger enol contributions than indigo.

Transfer integrals t were estimated from the (geometry non optimized) dimers (Table S4). Accordingly, the differences of HOMO and LUMO transfers are smaller than the frozen orbital approximation.[S4]

Table S1. Calculated HOMO and LUMO energies, HOMO/LUMO gaps (E_{HL}) and crystal and optimized bond distances (Å).

Compound		HOMO (eV)	LUMO (eV)	E_{HL} (eV)	Intermol. N−O	N−H O−H [a]	C=O
Indigo	Crystal [33]	−5.25	−3.28	1.97	2.861	0.951	1.268
	Crystal [34]	−5.57	−3.40	2.17	2.894	0.978	1.239
	Optimized	−5.52	−3.36	2.16		1.013	1.234
	Enol	−5.38	−4.16	1.22		1.013 [a]	1.317
DPh-indigo	Crystal [6]	−5.52	−3.44	2.08	3.079	0.860	1.238
	Optimized	−5.49	−3.42	2.07		1.013	1.234
	Enol	−5.38	−4.16	1.22		1.012 [a]	1.334
IBI	Optimized	−5.62	−3.18	2.44		1.011	1.223
	Enol	−5.31	−3.82	1.49		0.970 [a]	1.348
IB	Crystal A	−6.01	−3.40	2.61	2.913	0.860	1.288
	B				2.874		1.234
	C				2.961		1.247
	D				2.930		1.241
	Optimized	−6.01	−3.22	2.79		1.019	1.24
	Enol	−5.52	−3.69	1.83		0.969 [a]	1.347
C_nIB	Optimized	−5.80	−2.97	2.83		1.011	1.222
	Enol	−5.33	−3.45	1.88		0.970 [a]	1.350
Isoindigo	Crystal [35]	−5.94	−3.35	2.64	2.811	1.042	1.262
	Optimized	−5.94	−3.30	2.64		1.010	1.221
	Enol	−6.20	−3.58	2.62		0.976 [a]	1.345
TIIG	Crystal [15]	−5.44	−3.13	2.31	2.820	0.880	1.228
	Optimized	−5.38	−3.14	2.79		1.009	1.222
	Enol	−5.70	−3.53	2.17		1.136 [a]	1.223
Quinacridone	Crystal [41]	−5.72	−3.25	2.47	2.750	0.887	1.373
	Optimized	−5.57	−2.82	2.75		1.010	1.233
	Enol	−5.30	−3.29	2.01		0.969 [a]	1.357
BrNQH	Crystal [S5]	−5.34	−4.89	0.45	2.740		1.365
							1.237
	Optimized [b]	−5.83	−4.57	1.26		0.969 [a]	1.367
							1.225

[a] N−H for crystal and optimized, while O−H for enol.

[b] For independent hydroquinone and quinone molecules.

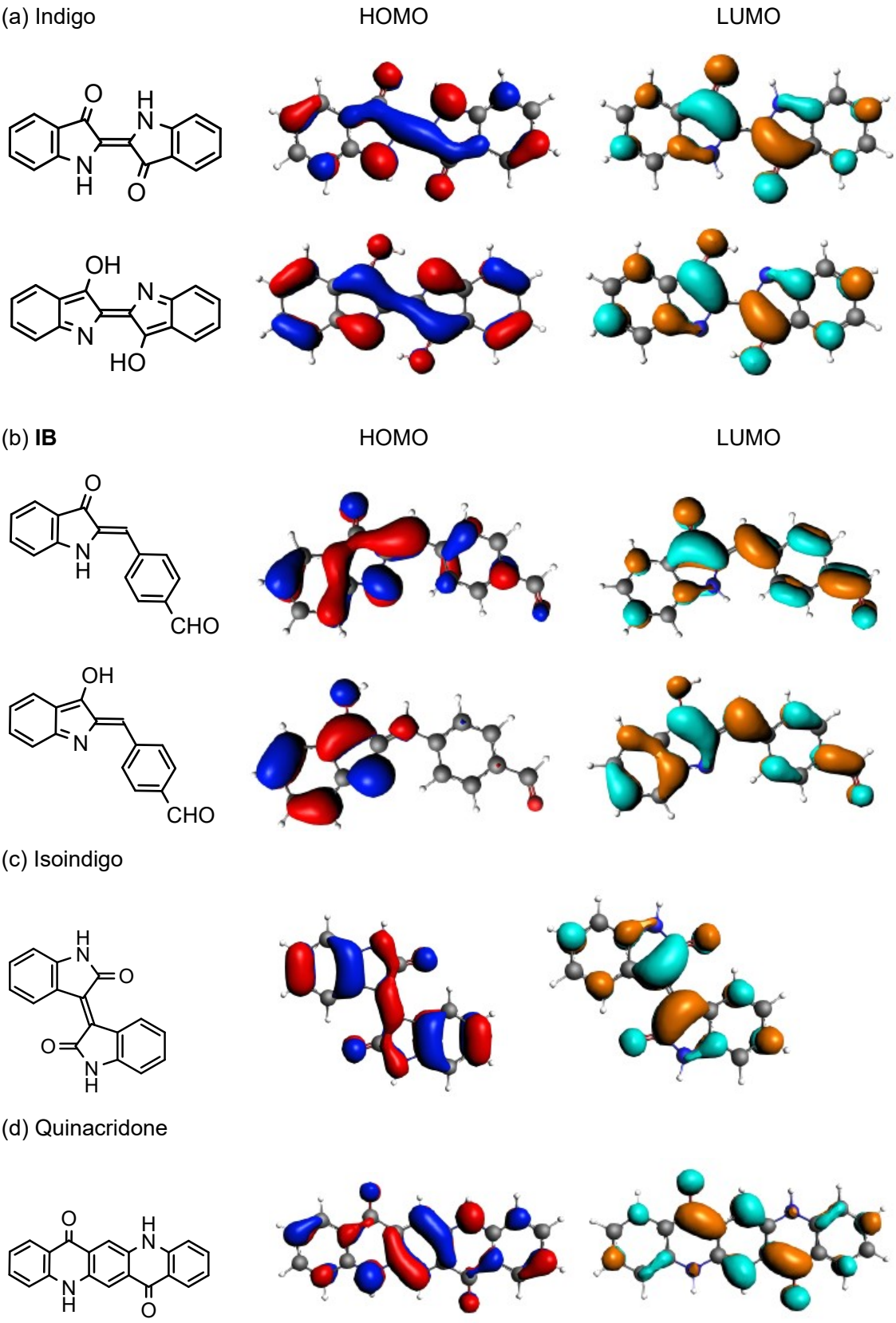

Fig. S2. HOMO and LUMO of (a) indigo, (b) **IB**, (c) isoindigo, and (d) quinacridone.

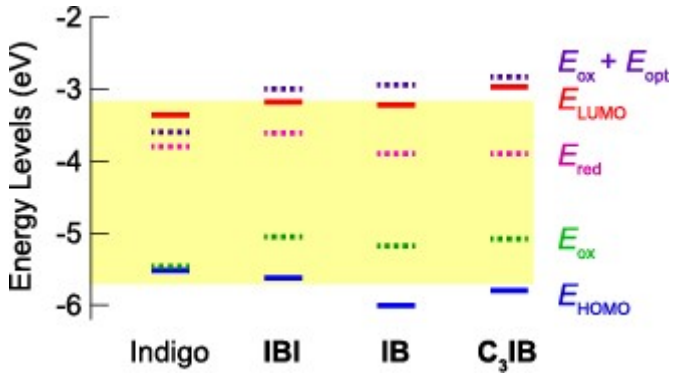

Fig. S3. Observed and calculated energy levels.

Table S2. Enol contributions (R_{enol}) estimated from the optical edge shift.

		E_1 /E_{HL}(eV)		E_{opt} (eV)		R_{enol}	
		keto	enol Intra (Inter)	DMF	Thin film	DMF	Thin film
Indigo	E_1	2.02	0.78	1.90	1.70	10%	26%
	E_{HL}	2.16	1.22 (0.38)			28% (15%)	49% (26%)
IBI	E_1	2.49	1.32	2.05	1.94	38%	47%
	E_{HL}	2.44	1.49			41%	53%
IB	E_1	2.74	0.80	2.24	2.14	26%	31%
	E_{HL}	2.79	1.83 (0.48)			57% (24%)	68% (28%)
C_3IB	E_1	2.77	1.48	2.24	2.21	41%	43%
	E_{HL}	2.83	1.88			62%	65%

Crystal Structures

Crystals for X-ray single-crystal structure analyses were obtained by sublimation of **IB**. The X-ray oscillation photographs were taken using a RIGAKU R-AXIS RAPID II imaging plate with Cu-$K\alpha$ radiation from a rotation anode source with a confocal multilayer X-ray mirror (RIGAKU VM-Spider, λ = 1.54187 Å). The crystallographic data are listed in Table S3. The structures were solved by the direct method (SIR2008) and refined by the full matrix least-squares procedure (SHELXL).[S6,S7] Anisotropic thermal parameters were adopted for all non-hydrogen atoms. Transfer integrals were estimated from the respective dimers.

Table S3. Crystallographic data of **IB**.

	IB
Formula	$C_{16}H_{11}NO_2$
Formula weight	249.27
Crystal System	monoclinic
Space Group	*Cc*
Shape	orange-plate
a (Å)	52.556(3)
b (Å)	3.8744(3)
c (Å)	24.2104(14)
α (deg)	90
β (deg)	103.315(3)
γ (deg)	90
V (Å^3)	4797.2(5)
Z-value	16
T (K)	262
D_{calc} (g cm^{-3})	1.380
Total reflns.	23433
Unique reflns. (R_{int})	4016 (0.1274)
R_1 [$F^2 > 2\sigma(F^2)$]	0.1152
wR_2 [All reflns.]	0.3500
GOF	1.043

Transfer integrals

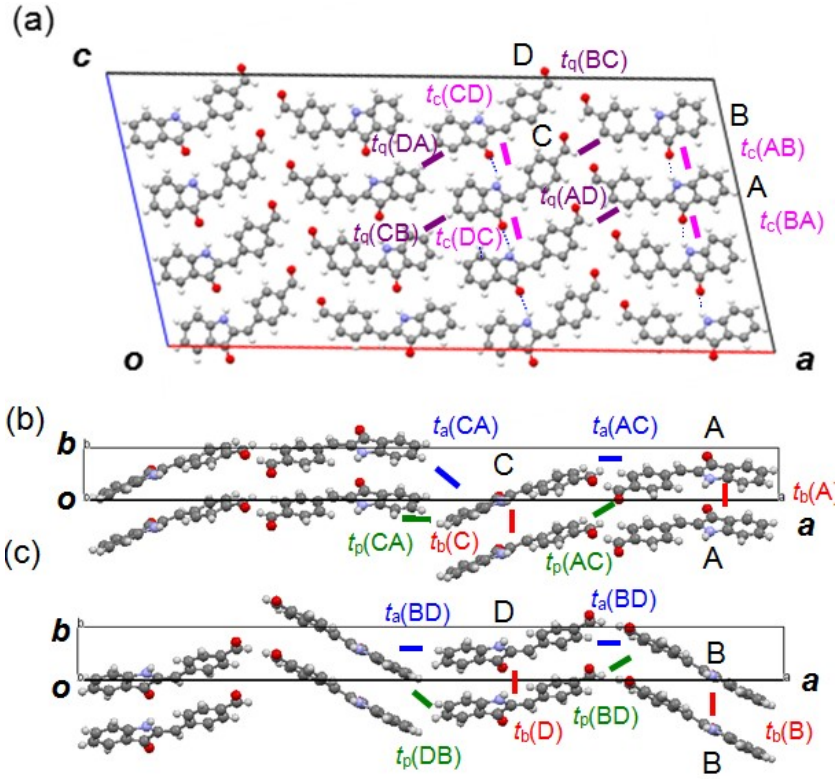

Fig. S4. Transfer integrals of **IB**.

Table S4. Calculated transfer integrals (meV) of **IB** for HOMO/LUMO.

	AA	BB	CC	DD
t_b	96/86	93/57	195/43	12/30
	AB	CD	BA	DC
t_c	34/8	38/6	63/17	38/4
	AC	BD	CA	DB
t_a	2/16	1/9	2/0	3/4
t_p	1/5	3/1	7/3	3/1
	BC	AD	DA	CB
t_q	1/3	2/19	5/11	0/3

Device fabrication

Thin-film transistors were fabricated onto n-doped Si substrates with a thermally-grown SiO_2 (300 nm, C = 11.5 nF/cm^2) dielectric layer. The SiO_2 surface was passivated with 20 nm thick layer of tetratetracontane ($C_{44}H_{90}$, TTC, ε = 2.5), by thermal deposition under a vacuum of 10^{-3} Pa.[S8–S10] The resulting overall capacitance of the gate dielectrics was 10.4 nF/cm^2.[S11] A 50 nm thick active layer was formed by thermal deposition under a vacuum of 10^{-3} Pa. The XRD and AFM measurements were done for these thin films. Then the top-contact electrodes were patterned by thermal deposition of Au or (TTF)(TCNQ) through a shadow mask; the channel had width W = 1000 μm and length L = 100 μm.[37] Au is a large work function metal (5.1 eV) preferable to hole injection, but also good for electron injection.[S12] Owing to the lack of the interfacial polarization, (TTF)(TCNQ) (~4.7 eV) shows low contact resistance both for hole and electron injection.[37,S12] OFET properties were measured using a Keithley 4200 semiconductor parameter analyzer under a vacuum of 10^{-3} Pa. The field-effect mobility μ and threshold voltage V_T were calculated in the saturation regime by using the equation, $I_{DS} = \mu(WC_i/(2L))(V_G - V_T)^2$, where I_{DS} is drain current and V_G is gate voltage; μ is extracted from the slope where the plot of $\sqrt{I_{DS}}$ *vs*. V_G is straight.

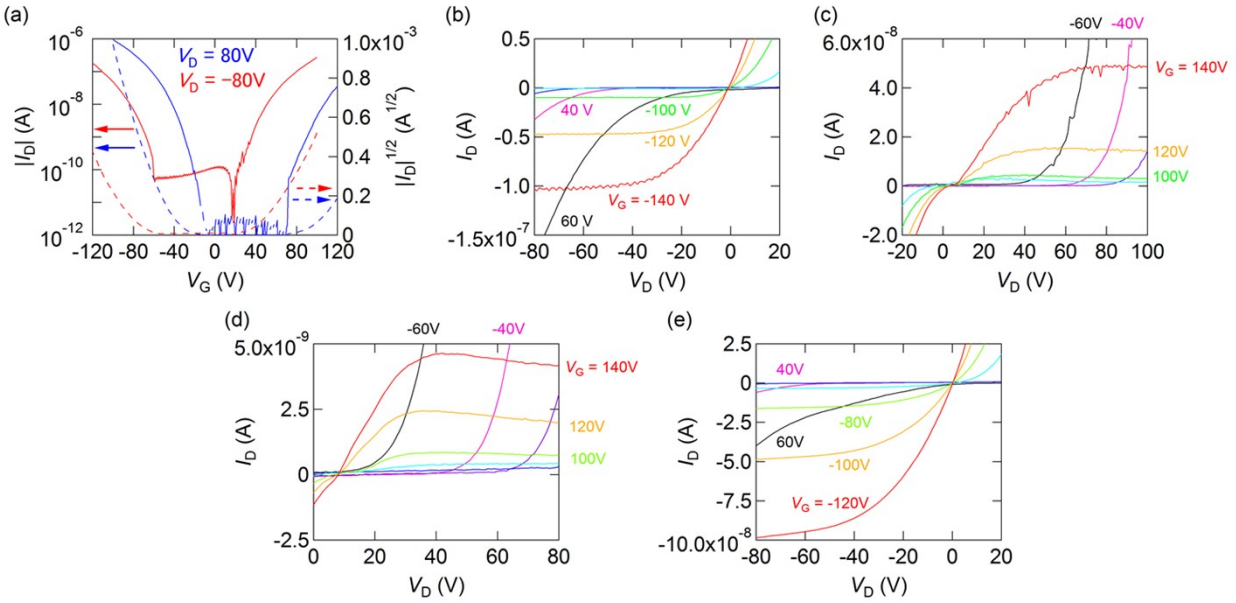

Fig. S5. (a) Transfer and (b)(c) output characteristics of **IBI** for gold electrodes. (d)(e) Output characteristics of **IBI** for (TTF)(TCNQ) electrodes.

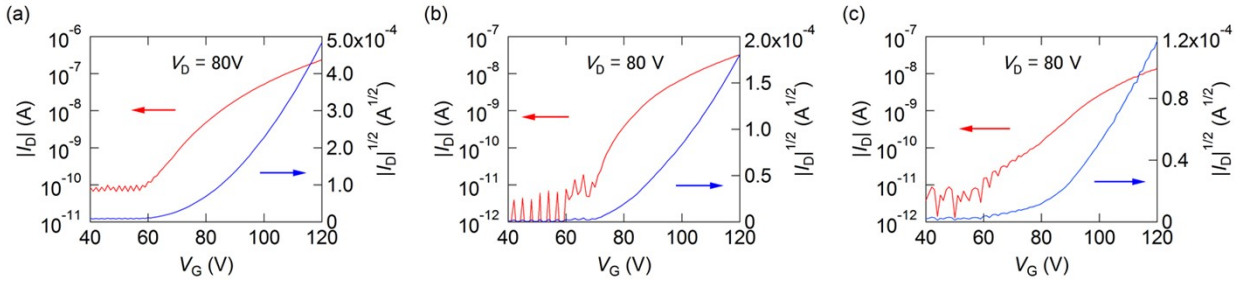

Fig. S6. (a) Transfer characteristics of **C_3IB, (b) C_6IB** and (c) **C_8IB** (gold electrodes).

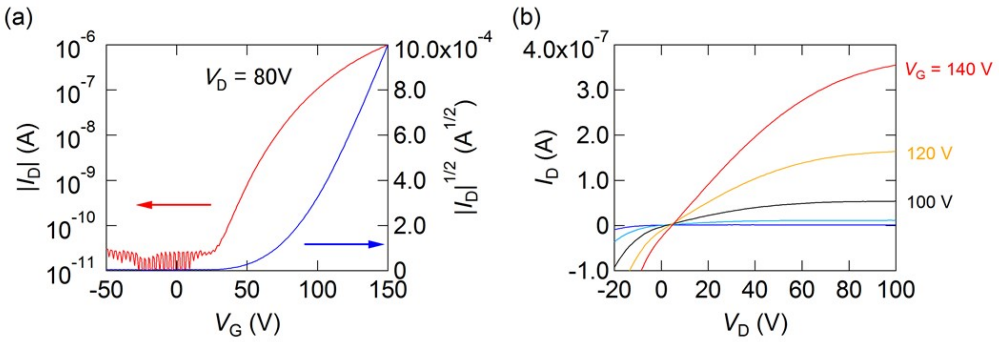

Fig. S7. (a) Transfer and (b) output characteristics of **EtPhIB** (gold electrodes).

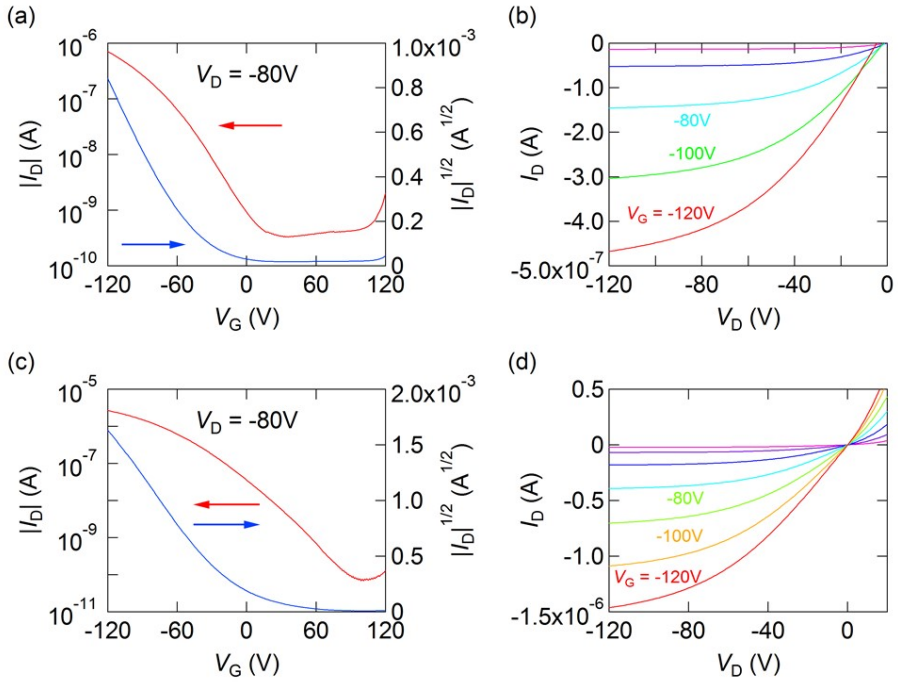

Fig. S8. (a) Transfer and (b) output characteristics of **IDT** (gold electrodes). (c) Transfer and (d) output characteristics of **IDT** ((TTF)(TCNQ) electrodes).

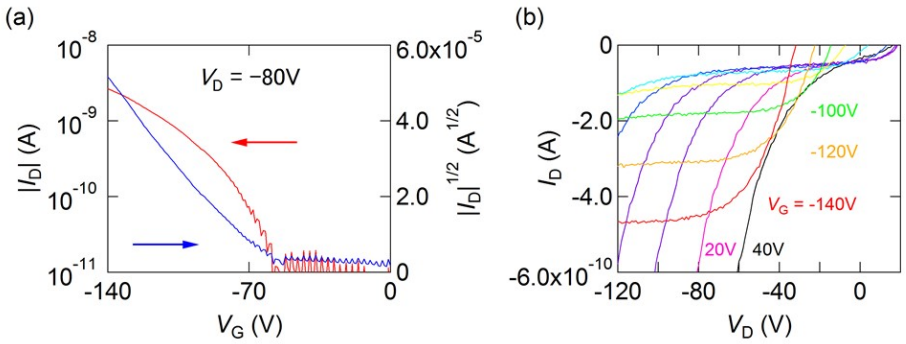

Fig. S9. (a) Transfer characteristics of **IDTI** (gold electrodes). (b) Output characteristics of **IDTI** ((TTF)(TCNQ) electrodes).

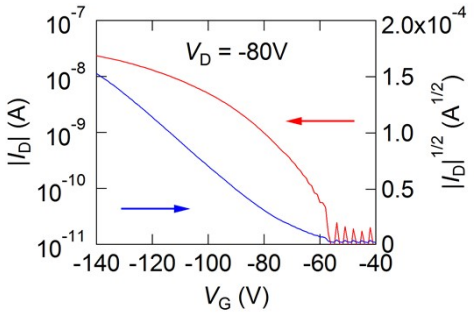

Fig. S10. Transfer characteristics of **Me-IGI** (gold electrodes).

Impact of proton transfer

To investigate the influence of hydrogen bond, the density functional calculations were performed with the B3LYP* functional and TZP basis set using ADF software.[28,S1] Since the phenomena are related to intermolecular interactions, BLYP-D3 is investigated as well,[S13] but the resulting potential curves are practically the same except for the near-core regions. In Fig. 6, the proton positions were moved starting from the original N−H position towards the oxygen atom, where all other atoms were taken from the crystal structures.[34,35,40] Intermolecular proton transfer was investigated from calculations of dimers. For intramolecular proton transfer of isoindigo, this method produces unreasonably short C−H distances in the intermediate region, so that the proton was moved from N−H to an expected O−H structure (Fig. S11(a)). The potential curves of DPh-indigo in Fig. S11(b) were estimated by omitting the phenyl groups.

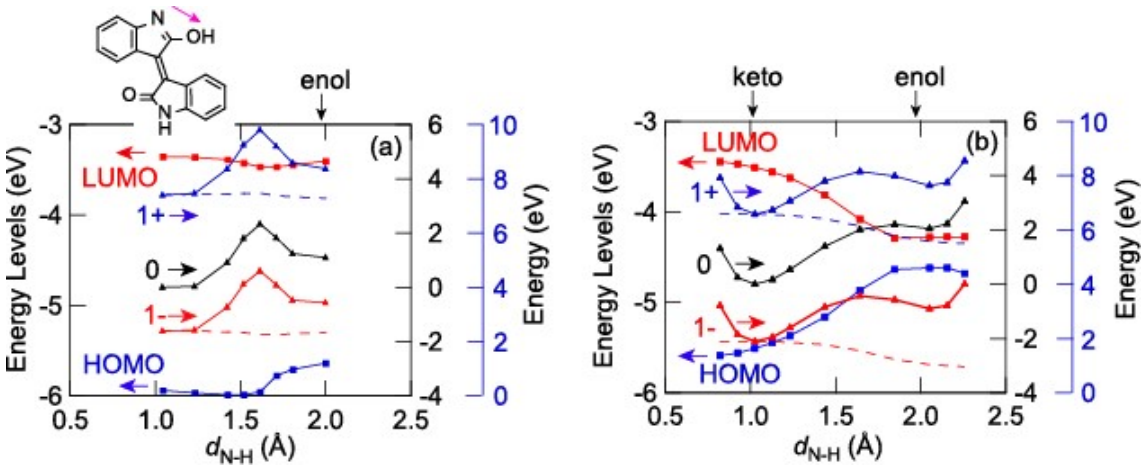

Fig. S11. (a) HOMO/LUMO levels and potential curves calculated as a function of $d_{N–H}$ for intramolecular 1H transfer of isoindigo. (b) HOMO/LUMO levels and potential curves calculated as a function of $d_{N–H}$ for intermolecular 1H transfer of DPh-indigo.[6]

Calculated mobilities

When the crystal structure is known, we can estimate mobilities by the Marcus theory[45]

$$\mu = \frac{1}{2n}\frac{ea^2}{k_B T}k \qquad k = \frac{2\pi t^2}{h}\sqrt{\frac{\pi}{\lambda k_B T}}\exp\left(-\frac{\lambda}{4k_B T}\right) \tag{S2}$$

where e is the elemental charge, a is the lattice spacing, k_B is the Boltzmann constant, and T is the temperature. Reorganization energies λ were evaluated from the energy differences between the neutral and ionic geometries.[45] Mobility values in Table S4 were calculated from eqn (S2) without considering the pathways.[S13] It has been pointed out that when the transfer integral t increases, the reorganization energy λ tends to increase, and the hole and electron mobilities are approximately the same in ambipolar transistors.[S4] As shown in Table S5, the present calculation also suggests ambipolar transport in DPh-indigo, isoindigo, **TIIG**, and **DPh-TIIG**. Although the mobilities are measured in evaporated films, these materials actually show ambipolar transistor properties.

When the hydrogen bond is blocked, naphthosemiquinone (**BNQ**, Table S5) affords similar λ and μ for hole and electron, and actually realizing balanced ambipolar transport.[S14] We have to also point out that the hydrogen-bonded materials have

considerable interchain transfers along the hydrogen bonds (Table S5), which are contrasting to the highly one-dimensional nature of the ordinary stacking structures in **BNQ**. It should be, however, kept in mind that transfers obtained from the dimer energy splitting may be influenced by the hydrogen bond. Reorganization energies of the enol forms are not largely different from those of the keto forms in indigo and **IB**.

Table S5. Calculated hole/electron mobilities for HOMO/LUMO.

Compound		HOMO/ LUMO (eV) [b]	*t* (meV) [c]	λ [d] (meV)	μ [e] ($cm^2 V^{-1} s^{-1}$)
Indigo	stack	−5.52/−3.36	73/67 (//*b*)	186/348	0.74/0.09
			29/11 (//*c*)	(240/256)	(0.01/0.01)
DPh-indigo [6]	brick	−5.49/−3.42	76/147 (//*b*+*c*)	134/309	1.07/0.49
	work		24/19 (//*c*)		(0.56/0.95)
IB	stack	−6.01/−3.22	99/54 (//*b*)	243/364	0.31/0.023
			43/9 (//*c*)	(350/320)	(0.0039/0)
Isoindigo [35]	brick	−5.94/−3.30	36/79 (//*a*+*b*)	238/410	0.076/0.053
	work		48/32 (//*a*)		(0.0072/0.0041)
TIIG [a 15]	stack	−5.38/−3.14	98/159 (//*b*)	281/330	0.17/0.44
			3/0 (//*a*+*b*)		(0.0016/0.0029)
DPh-TIIG [a 15]	brick	−5.49/−3.42	63/119(//*a*+*b*)	281/330	0.15/0.31
Quinacridone [40,41]	stack	−5.57/−2.82	94/11 (//*a*)	132/215	1.15/0.006
			53/24 (//*b*)		(0.2/0)
BNQ [S15 a]	stack	−5.31/−3.56	186/105 (//*a*)	342/300	0.49/0.25
			15/14 (//*b*)		(0.0018 /0.0012)

[a] **TIIG**: thienoisoindigo,[15] **DPh-TIIG**: diphenyl-**TIIG**,[15] and **BNQ**: 2,2'-dinaphthosemiquinone.[S15]

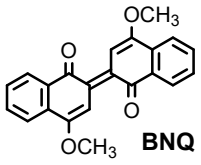

BNQ

[b] Calculations based on geometry optimized structures.

[c] Second transfers are in the inter-stacking direction with hydrogen bonds. Average of different stacks in **IB**.

[d] The values in the parentheses are reorganization energies of the enol forms.

[e] Observed mobilities in the parentheses.

References

S1 M. Reiher, O. Salomon and B.A. Hess, *Theor. Chem. Acc*. 2001, **107**, 48.

S2 Y. Zhao, D. G. Truhlar, *Theor. Chem. Acc*., 2008, **120**, 215.

S3 J. L. Brédas, *Mater. Horiz*., 2014, **1**, 17.

S4 H. Kojima and T. Mori, *Chem. Lett*., 2013, **42**, 68.

S5 K. Nakasuji, K. Sugiura, T. Kitagawa, J. Toyoda, H. Okamoto, K. Okaniwa, T. Mitani, H. Yamamoto, I. Murata, A. Kawamoto, J. Tanaka, *J. Am. Chem. Soc*., 1991, **113**, 1862.

S6 G. M. Sheldrick, *Acta Crystallogr. A*, 2015, **71**, 3.

S7 G. M. Sheldrick, *Acta Crystallogr. C*, 2015, **71,** 3.

S8 M. Kraus, S. Richler, A. Opitz, W. Brütting, S. Haas, T. Hasegawa, A. Hinderhofer and F. Schreiber, *J. Appl. Phys*., 2010, **107**, 094503.

S9 M. Kraus, S. Haug, W. Brütting and A. Opitz, *Org. Electron*., 2011, **12**, 731.

S10 A. Opitz, M. Horlet, M. Kiwull, J. Wagner, M. Kraus and W. Brütting, *Org. Electron*., 2012, **13**, 1614.

S11 K. J. Baeg, Y. Y. Noh, J. Ghim, B. Lim and D. Y. Kim, *Adv. Funct. Mater*., 2008, **18**, 3678.

S12 H. Wada, K. Shibata, Y. Bando and T. Mori, *J. Mater. Chem*., 2008, **18**, 4165.

S13 S. Grimm, *WIREs Comp. Mol. Sci*., 2011, **1**, 211.

S14 S.-H. Wen, A. Li, J. Song, W.-Q. Deng, K.-L. Han and W. A. Goddard III, *J. Phys. Chem. B*, 2009, **113**, 8813.

S15 T. Higashino, S. Kumeta, S. Tamura, Y. Ando, K. Ohmori, K. Suzuki and T. Mori, *J. Mater. Chem. C*, 2015, **3**, 1588.